Neurobiology of Aging 84 (2019) 240.e13–240.e22

Contents lists available at ScienceDirect

Neurobiology of Aging

journal homepage: www.elsevier.com/locate/neuaging

Tau aggregation and seeding analyses of two novel *MAPT* variants found in patients with motor neuron disease and progressive parkinsonism

Sachiko Nakayama [a], Shotaro Shimonaka [b,c], Montasir Elahi [a,b], Kenya Nishioka [a], Yutaka Oji [a], Shin-Ei Matsumoto [d], Yuanzhe Li [a,b], Hiroyo Yoshino [c], Kaoru Mogushi [e], Taku Hatano [a], Takeshi Sato [f], Teikichi Ikura [g], Nobutoshi Ito [g], Yumiko Motoi [a,b], Nobutaka Hattori [a,b,c,*]

[a] Department of Neurology, Juntendo University, School of Medicine, Tokyo, Japan
[b] Department of Diagnosis, Prevention and Treatment of Dementia, Juntendo University, Graduate School of Medicine, Tokyo, Japan
[c] Research Institute for Diseases of Old Age, Juntendo University, Graduate School of Medicine, Tokyo, Japan
[d] Department of Immunology, Kagoshima University, Graduate School of Medical and Dental Sciences, Kagoshima, Japan
[e] Diagnostics and Therapeutics of Intractable Diseases, Intractable Disease Research Center, Juntendo University School of Medicine, Tokyo, Japan
[f] Section of Neurology, Nanohana Clinic, Tokyo, Japan
[g] Department of Structural Biology, Tokyo Medical and Dental University (TMDU), Medical Research Institute, Tokyo, Japan

ARTICLE INFO

Article history:
Received 10 March 2018
Received in revised form 22 February 2019
Accepted 22 February 2019
Available online 1 March 2019

Keywords:
Genetics
Microtubule-associated protein tau
Parkinsonism
Frontotemporal dementia
Motor neuron disease

ABSTRACT

Variants in the microtubule-associated protein tau (*MAPT*) gene cause the genetic tauopathies, a subgroup of frontotemporal dementia (FTD) disorders. Through genetic screening of 165 cases possibly associated with tauopathies, including 88 Alzheimer's disease, 26 behavioral variant FTD, eight primary progressive aphasia, nine FTD with motor neuron disease, 21 progressive supranuclear palsy, and 13 corticobasal syndrome, we identified two novel *MAPT* variants: a heterozygous missense variant, *p*.P160S, in a patient with FTD with motor neuron disease and a heterozygous insertional variant, *p*.K298_H299insQ, in three patients with familial progressive supranuclear palsy. The corresponding recombinant tau proteins showed reduced microtubule assembly and increased aggregation by thioflavin S assay. Exon trapping analysis showed that *p*.K298_H299insQ resulted in the overproduction of 4-repeat tau. In a cell-based model, *p*.K298_H299insQ had both a higher aggregation ability and seeding activity compared with wild-type tau. These findings indicate that both *p*.P160S and *p*.K298_H299insQ may relate to neurodegeneration.

1. Introduction

Frontotemporal dementia (FTD) or frontotemporal lobe degeneration (FTLD) is characterized by personality changes, language impairment, and a deficit in executive functions (Rascovsky et al., 2011). Recent robust advances in molecular genetics uncovered association between several types of pathogenic variants and FTD, especially in familial cases. In Caucasians, 20%–50% of patients with FTD have a family history. Known genes with pathogenic variants include *microtubule-associated protein tau* (*MAPT*), *granulin precursor* (*GRN*), and *chromosome 9 open reading frame 72* (*C9orf72*), found in 60% of cases of familial FTD, and *valosin-containing protein*, *chmp family*, *member 2B* (*CHMP2B*), and *fused in sarcoma* (*FUS*), seen in rare cases (less than 5%) (Olszewska et al., 2016). In contrast, Japanese patients with FTD have a low prevalence of family history (9.5%–20%), few identified genetic factors (less than 5% in total), and 1.5% of cases with *MAPT* variants (Ng, 2015; Wada-Isoe et al., 2012).

MAPT is localized in chromosome 17q21 and encodes the MAPT. The human central nervous system contains six tau isoforms, including R1–R4, with three isoforms having four repeats (4R) each and three having three repeats (3R) each. These isoforms are expressed in the adult human brain and are produced by alternative splicing of messenger RNA transcripts. Although more than 53 different *MAPT* variants have been detected, including missense, deletion, and silent variants, pathogenic variants in *MAPT* are highly

* Corresponding author at: Department of Neurology, Juntendo University, School of Medicine, 2-1-1 Hongo, Bunkyo-ku, Tokyo 113-8421, Japan. Tel.: +81 3 3813 3111; fax: +81 3 5800 0547.
E-mail address: nhattori@juntendo.ac.jp (N. Hattori).

0197-4580/$ – see front matter © 2019 Elsevier Inc. All rights reserved.
https://doi.org/10.1016/j.neurobiolaging.2019.02.016

concentrated in exons 9–12 that encode the repeats (R1–R4) in the carboxy-terminal domain (Wang and Mandelkow, 2016). The microtubule-binding domain (MBD), which comprises the repeats and flanking regions (residues 243–372), is considered to be responsible for microtubule interactions or aggregation (Mukrasch et al., 2005). Recently, in non-MBD regions in *MAPT*, *p*.A152T in exon 7 was identified as a risk for FTD-spectrum disease and Alzheimer's disease. Functional analysis showed that *p*.A152T reduces microtubule binding affinity and increases the formation of tau oligomers (Coppola et al., 2012). Induced pluripotent stem cells carrying *p*.A152T show increased formation of tau fragments and phosphorylated tau, resulting in axonal degeneration in vitro (Fong et al., 2013). Transgenic mice harboring *p*.A152T show severe neuronal loss in the hippocampus (Maeda et al., 2016). The behavior of this variant suggests that the regions outside MBD may have an important role in the normal function of tau.

FTLD has heterogeneous clinical manifestations. FTLD-tau is characterized by deposition of abnormally modified tau inclusions in neuronal and glial cells. FTLD-tau with *MAPT* variants presents various types of neurodegenerative disorders: behavioral variant frontotemporal dementia (bvFTD), primary progressive aphasia (PPA), atypical parkinsonism such as progressive supranuclear palsy (PSP) and corticobasal degeneration syndrome (CBS), and rarely motor neuron disease (MND) (Di Fonzo et al., 2014; Forrest et al., 2018; Irwin et al., 2015). FTLD-tau with *p*.R406W in *MAPT* shows late onset and slowly progressive dementia, clinically diagnosed with Alzheimer's disease (Lindquist et al., 2008).

In this study, we identified two novel variants in *MAPT* after genetic screening of 165 Japanese patients who clinically associated with tauopathies and functionally characterized the corresponding variant proteins. Our findings will expand the genotype-phenotype associations of *MAPT* and improve our understanding of tau pathogenesis.

2. Materials and methods

2.1. Subjects

All patients and caregivers were fully informed of the details of the study and provided written consent to participate. The study protocol was approved by the Committee for Ethics in Clinical Research of the Juntendo University School of Medicine. We studied 165 Japanese patients possibly associated with tauopathies with or without a family history of disease (Supplementary Table 1). All subjects were clinically diagnosed with Alzheimer's disease, bvFTD, PPA, PSP, and CBS according to corresponding internal consensus criteria (American Psychiatric Association, 2013; Gorno-Tempini et al., 2011; Litvan et al., 1996; Mathew et al., 2012; Rascovsky et al., 2011). FTD-MND was diagnosed by needle electromyogram using the standard criteria for MND (de Carvalho et al., 2008). The autosomal dominant mode of inheritance was defined as having one or more first-degree family members with the same symptoms. The demographic information of the 165 enrolled patients is shown in Supplementary Table 1. The study population included cases of Alzheimer's disease ($n = 88$), bvFTD ($n = 26$), FTD-MND ($n = 9$), PPA ($n = 8$), PSP ($n = 21$), and CBS ($n = 13$). The average age at examination was 68.0 ± 10.1 years (±standard deviation). The average age at disease onset was 63.9 ± 11.1 years.

2.2. Genetic analysis

Genomic DNA was isolated from peripheral blood using the QIAamp blood Maxi Kit (Qiagen, Hilden, Germany). All coding exons and their flanking introns of *MAPT* were amplified using polymerase chain reaction (PCR). PCR primer and conditions are described in the Supplementary material and methods. After purification of PCR amplicons using ExoSAP IT (GE Healthcare, Little Chalfont, UK), direct sequencing was carried out using the Big Dye Terminator v3.1 Cycle Sequencing Kit (Life Technologies, Foster City, CA, USA) and a 3130 Genetic Analyzer (Life Technologies).

The sequencing results were compared with the *MAPT* reference sequence (*MAPT*; RefSeq accession number NM_005910.5). Pathogenicity of the identified variants was analyzed using prediction tools or public gene databases such as PolyPhen-2 (Adzhubei et al., 2010), MutationTaster (Schwarz et al., 2014), combined annotation-dependent depletion (CADD) (Kircher et al., 2014), and rare exome variant ensemble learner (Ioannidis et al., 2016). Variant frequencies were investigated using the ExAC database (Lek et al., 2016) and Human Genetic Variation Database for the Japanese population (Higasa et al., 2016). Evolutionary conservation of the mutated amino acids was evaluated using NCBI gene HomoloGene (https://www.ncbi.nlm.nih.gov/homologene/).

2.3. Biochemical analysis

2.3.1. Purification of recombinant tau

Human tau complementary DNA (cDNA) in the bacterial expression plasmid pRK172 was used to produce recombinant proteins (Matsumoto et al., 2015). Quikchange site-directed mutagenesis kit (StrataGene, La Jolla, CA, USA) was used to change proline to serine at position 160 and insert adenine-cytosine-adenine after nucleotide 896. All sequences were verified by DNA sequencing. Tau proteins were expressed in *Escherichia coli* BL21 (DE3) and purified as described previously (Hasegawa et al., 1997). Recombinant tau proteins were designated as recombinant 2N4R, 2N4R-P160S, and 2N4R-insQ.

2.3.2. Microtubule assembly assay and exon trapping analysis

Recombinant tau proteins (5 μM) were incubated with 30 μM porcine brain tubulin (Cytoskeleton, Denver, CO, USA) in assembly buffer [80 mM piperazine-N,N'-bis(2-ethanesulfonic acid (pH 6.8), 1 mM $MgCl_2$, 1 mM ethylene glycol tetraacetic acid, 1 mM dithiothreitol (DTT), and 10% glycerol] at 37 °C. Assembly of tubulin into microtubules was monitored over time using absorbance change at 340 nm in a Spectramax 250 Microplate Reader (Molecular Devices, USA). Four assays were performed for each of the three recombinant tau protein variants.

For exon trapping analysis, the exon trapping vector pSPL3 with the wild-type tau sequence was used. The wild-type construct contained exon 10 as well as 34 nucleotides of upstream intronic sequence and 85 nucleotides of downstream intronic sequence (kindly provided by Dr Hasegawa). The Quikchange site-directed mutagenesis kit (StrataGene) was used to introduce variants *p*.K298_H299insQ and *p*.N279K in exon 10. *p*.N279K was used as a positive control. COS-7 cells were transfected using 1 μg/well of plasmid DNA with Xtreme Gene9. Transfected cells were cultured for 24 hours and total RNA was isolated and used for cDNA synthesis. The cDNA was amplified using PCR, and the proportion of exon 10–containing transcripts was determined using image analysis of photographs of agarose gel electrophoresis of PCR products, as described previously (Hasegawa et al., 1999). Three independent experiments were performed for each construct.

2.3.3. Heparin-induced tau aggregation assay and electron microscopy

Recombinant 2N4R (20 μM) and its variants were incubated in 30 mM Tris-HCl (pH 7.5) containing 0.1 mg/mL heparin, 0.1% sodium azide, and 20 mM DTT with shaking at 37 °C. Aliquots of 10 μL of assembly mixtures were mixed with 200 μL of 20 mM 3-(N-morpholino)propanesulfonic acid buffer containing 5 μM thioflavin

S (ThS). After 30 minutes of incubation at 25 °C, the samples were loaded into a 96-well black plate. ThS fluorescence was measured at various time points using a FlexStation II (Molecular Devices, Sunnyvale, CA, USA) (set at 436 nm excitation/535 nm emission). Three independent experiments were performed for each construct.

To obtain sarkosyl (Sar)-insoluble pellet, 10-μL aliquots of sample were mixed with 30 mM Tris-HCl containing 1% Sar. After incubation for 30 minutes on ice, the mixture was centrifuged at 100,000*g* for 20 minutes at 4 °C, and the supernatant was recovered. The remaining pellets were lysed in sodium dodecyl sulfate (SDS) buffer and heated at 100 °C for 5 minutes to prepare the Sar-insoluble pellet. Sar-insoluble pellets were subjected to SDS–polyacrylamide gel electrophoresis (SDS-PAGE) and stained with Coomassie Brilliant Blue. Three independent experiments were performed for each construct.

For electron microscopy analysis of tau filament formation, purified recombinant tau protein (15 μM) and heparin (0.1 mg/mL) were incubated at 37 °C for 7 days in 300 μL of 30 mM Tris-HCl, pH 7.5, containing 0.1% sodium azide and 20 mM DTT. Carbon-formvar grids were placed on top of a 2-μL drop of the diluted samples for 1 minute and then stained with 2% phosphotungstate for 60 seconds. Micrographs were recorded on a transmission electron microscope (HT7700, Hitachi, Tokyo, Japan).

2.3.4. Far ultraviolet circular dichroism spectroscopy

The secondary structural change during heparin-induced aggregate formation was monitored using far ultraviolet circular dichroism (CD) spectroscopy. CD measurements were carried out using 10 μM recombinant 2N4R, 2N4R-P160S, and 2N4R-insQ in 10 mM Tris-HCl buffer (pH 7.5), heparin (0.1 mg/mL), and 1.0 mM tris(2-carboxyethyl)phosphine as reducing agent with a 2.0 mm cuvette and a JASCO J-815 spectropolarimeter (Jasco, Japan) as previously reported (Elahi et al., 2014). For each measurement the response time was 5 seconds and measurement temperature was 37 °C. In each experiment, three spectra were summed and averaged. For time-dependent analysis of spectral change of heparin-induced aggregation, recombinant tau was incubated at 37 °C with shaking and CD was recorded at 24, 48, 72, 96, and 120 hours. Secondary structural contents were analyzed using JASCO analysis software and were verified using the K2D3 web server and 41 CD values ranging from 200 to 240 nm (Andrade et al., 1993).

2.3.5. Cell culture seeding assay

For preparation of tau seed, purified recombinant tau protein (15 μM) and heparin (0.1 mg/mL) were incubated at 37 °C in 300 μL of 30 mM Tris-HCl, pH 7.5, containing 0.1% sodium azide and 10 mM DTT for 7 days with continuous shaking, and centrifuged at 100,000*g* for 20 minutes at 4 °C. The pellets were resuspended in 100 μL of phosphate-buffered saline and sonicated for 10 seconds. This preparation was used as seeds.

SH-SY5Y cells were cultured in Dulbecco's modified Eagle medium/F-12 medium (Sigma, St. Louis, MO, USA) with 10% fetal bovine serum and maintained at 37 °C in a humidified atmosphere of 5% CO_2. Wild-type human tau was overexpressed in SH-SY5Y cells by transfection with 1 μg/well of the pcDNA3.1 constructs encoding human full-length 2N4R (tau 1–441), 2N4R-P160S, and 2N4R-insQ using X-tremeGENE9 DNA transfection reagent (Roche, Germany). Cells were incubated for 16 hours, and then 2 μg/well of 2N4R, 2N4R-P160S, or 2N4R-insQ seeds was introduced using MultiFectam (Promega). After 24 hours of incubation in a CO_2 incubator, the medium was changed to fresh medium and culture was incubated for 48 hours.

Cells were harvested in A68 buffer (10 mM Tris-HCl (pH 7.5), 10% sucrose, 0.8 M NaCl, and 1 mM ethylene glycol tetraacetic acid) containing 1% Sar. Cell lysate was centrifuged at 100,000*g* for 20 minutes at 4 °C, the supernatant was recovered as the Sar-soluble fraction, and the protein concentration was determined using Pierce bicinchoninic acid protein assay kit (Thermo Scientific, MA, USA). The remaining pellets were lysed in SDS buffer and heated at 100 °C for 5 minutes to prepare the Sar-insoluble pellet. Both Sar-soluble fractions and Sar-insoluble pellets were analyzed using immunoblotting with T46 antibody (which recognizes a phosphorylation-independent epitope in amino acids 404–441; Invitrogen). Three independent experiments were performed for each construct.

For immunofluorescence microscopy, cell culture seeding assays were performed on collagen-coated coverslips and the cells were stained as described previously (Nonaka et al., 2010). Briefly, cells on the coverslips were incubated with PHF-1 (1:1000, a gift of Dr P. Davies, Albert Einstein College of Medicine, New York, USA), MC1 (1:500, a gift of P. Davies, Albert Einstein College of Medicine), AT8 (1:1000, Innogenetics, Zwijndrecht, Belgium), tauC (1:10,000, a gift of K. Ishiguro), and anti–α-tubulin (1:500, Bio-Rad, Hercules, CA, USA), followed by Alexa Fluor 488–conjugated goat anti-mouse IgG secondary antibody (1:500, Life Technologies, Carlsbad, CA, USA) and Alexa Fluor 555–conjugated goat anti-rabbit IgG secondary antibody (1:500, Life Technologies). 4′,6-Diamidino-2-phenylindole dihydrochloride staining was used to visualize the nuclei (Life Technologies). Fluorescence was evaluated using a fluorescence microscope (Apo Tome.2, Zeiss, Oberkochen, Germany). Each experiment was repeated three times and cells were counted in three views for each experiment.

2.3.6. Statistical analysis

Statistical analyses were performed using the JMP8 software (SAS Institute Japan). Unpaired Student's *t* test was used for comparison between two sample groups. For exon trapping analysis, the Mann-Whitney *U* test was performed. A p value of <0.05 was considered to be significant.

3. Results

3.1. Identification of two novel MAPT variants

Sequence analysis of the Japanese patients identified two novel *MAPT* variants: c.478C>T, *p*.P160S, in exon 7 of subjects from family A, and c.896_897insACA, *p*.K298_H299insQ, in exon 10 of subjects from family B (Fig. 1A–C and B and C, respectively). The clinical details are presented in Supplementary Table 2. Variant p.P160S was classified as "benign" in PolyPhen-2, MutationTaster, and rare exome variant ensemble learner (>0.55 indicates a high probability of disease variant). However, it was predicted to be "possibly deleterious" by CADD (between 10 and 20 means that a variant is among the top 10% of deleterious variants) and "not found" in ExAC and Human Genetic Variation Database. Variant p.K298_H299insQ was classified as possibly deleterious in CADD (Supplementary Table 3). The proline at position 160 is conserved among three species (Supplementary Fig. 1).

3.2. Case presentation

3.2.1. Family A: FTD-MND patient with the p.P160S MAPT variant

A 42-year-old, right-handed woman, the proband (Fig. 1C, II-2), noticed clumsiness in her right arm along with progressive gait disturbances that did not respond to levodopa. At age 47 years, the limbs were affected bilaterally, and she used a wheelchair all day. At age 49 years, her spontaneous speech was less fluent and dysarthric. She showed muscle weakness and spasticity in the upper and lower limbs, predominantly on the right side. Her index on the Mini-Mental State Examination was 30/30, but disinhibition, anosodiaphoria, and obsessive behavior were prominent. Atrophic

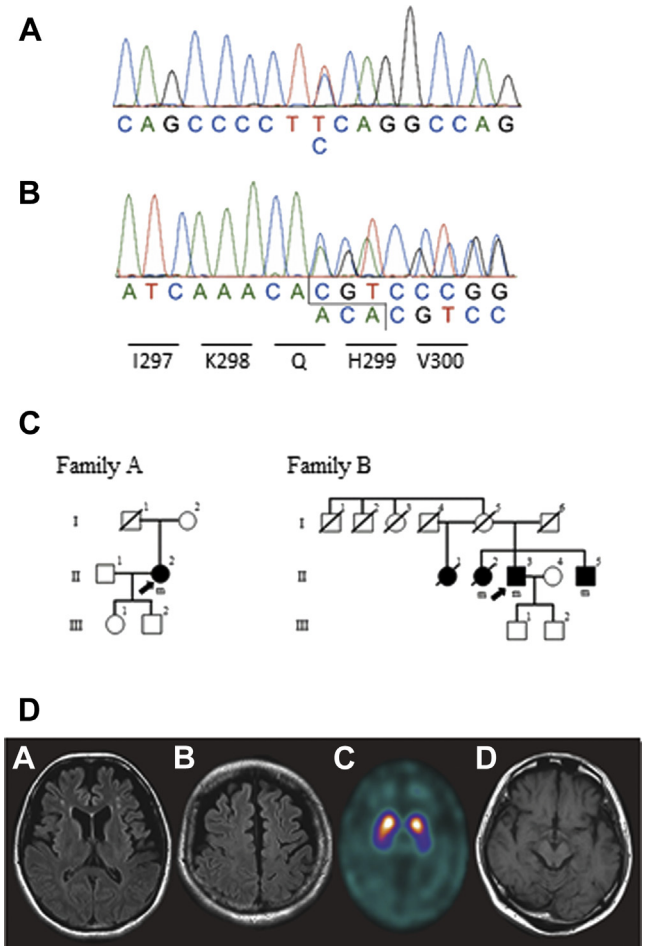

Fig. 1. Sequencing chromatogram, family pedigrees, and neuroimaging with two novel *MAPT* variants. (A and B) Sequencing chromatogram of II-2 shows the C to T variant (*p*.P160S) (A) and that of II-3 shows the ACA insertional variant (*p*.K298_H299insQ) (B). (C) II-2 in family A harboring variant *p*.P160S is the proband. Three patients of family B harbored variant *p*.K298_H299insQ: II-2, II-3, and II-5. (Arrow) proband; (square) male; (circle) female; (slashed circle) deceased; (filled circle) affected; and (m) mutation positive. (D) Neuroimaging—(A and B) axial fluid attenuation inversion recovery MRI of patient II-2 in family A with variant *p*.P160S showing asymmetric atrophy (left > right) of the frontal and temporal lobes and some hyperintensity lesions in the frontal white matter; (C) [^{123}I]FP-CIT single photon emission computed tomography of II-2 in family A; (D) Brain MRI of the proband, II-3 in family B. Abbreviations: ACA, adenine-cytosine-adenine; MAPT, microtubule-associated protein tau; MRI, magnetic resonance imaging.

changes were observed in the frontotemporal lobes on magnetic resonance imaging of brain (Fig. 1D-A and B). A needle electromyogram revealed acute denervation in the muscles of the sternocleidomastoid and first dorsal interosseous, matching the standard criteria of probable amyotrophic lateral sclerosis (de Carvalho et al., 2008). She was thus diagnosed with FTD-MND. At age 51 years, she was admitted to Juntendo University Hospital. She exhibited decreasing eye blink, vertical and horizontal gaze palsy, smooth pursuit abnormality, pseudobulbar palsy, and severe weakness in the upper and lower limbs. Her deep tendon reflexes were brisk. Brain single-photon emission computed tomography revealed hypoperfusion in the precentral regions, predominantly on the left side. The dopamine transporter densities of [^{123}I]N-ω-fluoropropyl-2β-carbomethoxy-3β-(4-iodophenyl) tropane single-photon emission computed tomography imaging disclosed a severe decrease in the left posterior putamen (Fig. 1D-C). One of her children had mental retardation with trisomy of chromosome 19 (Fig. 1C, III-1).

3.2.2. *Family B: PSP patient with the p.K298_H299insQ* MAPT *variant*

A 60-year-old male, the proband (Fig. 1C, II-3), noticed neck stiffness and decreasing eye blink. Neurologic examination demonstrated truncal rigidity, gait disturbance, and akinesia resistant to levodopa treatment. Two years later, postural instability and frequent falling became prominent. At age 66 years, he was diagnosed with PSP. The cognitive function indices were 30/30 and 17/18 in the Mini-Mental State Examination and Frontal Assessment Battery, respectively. However, his index according to the Japanese version of the Montreal Cognitive Assessment was 24/30, along with mildly impaired word fluency. These results matched with mild cognitive impairment. He exhibited bilateral ptosis, vertical gaze palsy, ptyalism, and bradykinesia in the trunk. Magnetic resonance imaging of brain revealed atrophy of the frontotemporal cortexes and midbrain tegmentum (Fig. 1D-D). His diagnosis matched the criteria of PSP. According to family members, two elder sisters (Fig. 1C, II-1 and II-2) and one younger brother (Fig. 1C, II-5) presented gait disturbance. Two brothers (Fig. 1C, II-3 and II-5) were clinically diagnosed with PSP, presenting mild cognitive decline in neuropsychological assessments performed approximately 5 years after the onset of motor symptoms. Two sisters (Fig. 1C, II-1 and II-2) also manifested cognitive decline during their lives. We detected *p*.K298_H299insQ in one sister, the proband, and one brother in family B (Fig. 1C, II-2, II-3, and II-5).

3.3. *Effects of* MAPT *variants on microtubule assembly and alternative splicing*

To investigate the functional effects of these tau variants, recombinant 2N4R, 2N4R-P160S, and 2N4R-insQ were evaluated in microtubule assembly assays. The results showed a reduced rate and extent of tubulin polymerization compared with 2N4R (Fig. 2A). The initial polymerization rate decreased to approximately 30% and 40% for 2N4R-P160S and 2N4R-insQ, respectively, compared with 2N4R. We also observed an 18% and 20% reduction in 2N4R-P160S and 2N4R-insQ, respectively, in the extent of microtubule assembly.

Exon trapping analysis was conducted to investigate the effect of the *p*.K298_H299insQ on splicing of exon 10—containing transcripts using the *p*.N279K as a positive control. The results were expressed as the ratios of exon 10—containing over exon 10—lacking transcripts (Fig. 2B). *p*.K298_H299insQ showed a significantly increased ratio of 4R/3R compared with wild-type constructs, with similar results to those of the *p*.N279K ($p < 0.05$).

3.4. *Effects of* MAPT *variants on heparin-induced tau aggregation*

The effects of *MAPT* variants on heparin-induced tau aggregation were investigated. Recombinant 2N4R-P160S and 2N4R-insQ showed a marked increase in ThS fluorescence from 24 to 72 hours compared with 2N4R (Fig. 2C). ThS fluorescence levels of 2N4R-insQ (Fig. 2C) were higher than those of 2N4R-P160S (Fig. 2C) at 24 hours, whereas the levels of 2N4R-P160S (Fig. 2C) gradually increased at 72 hours, exceeding those of 2N4R-insQ (Fig. 2C). The Sar-insolubility pattern of tau in SDS-PAGE was consistent with the ThS assay results (Fig. 2D). Electron microscopy analysis revealed that recombinant tau aggregates were mostly constituted of filamentous tau. The tau filaments were straight and smooth for 2N4R. In contrast, the majority of 2N4R-P160S filaments showed a wave-like shape and a diameter of ~20 nm, although a few percent of them were straight (Fig. 2E). Similar wavy filaments were also observed for 2N4R, although the wavy filaments of 2N4R-P160S were longer and more frequent. In contrast, 2N4R-insQ filaments were exceedingly short and flexible, with small and round shaped

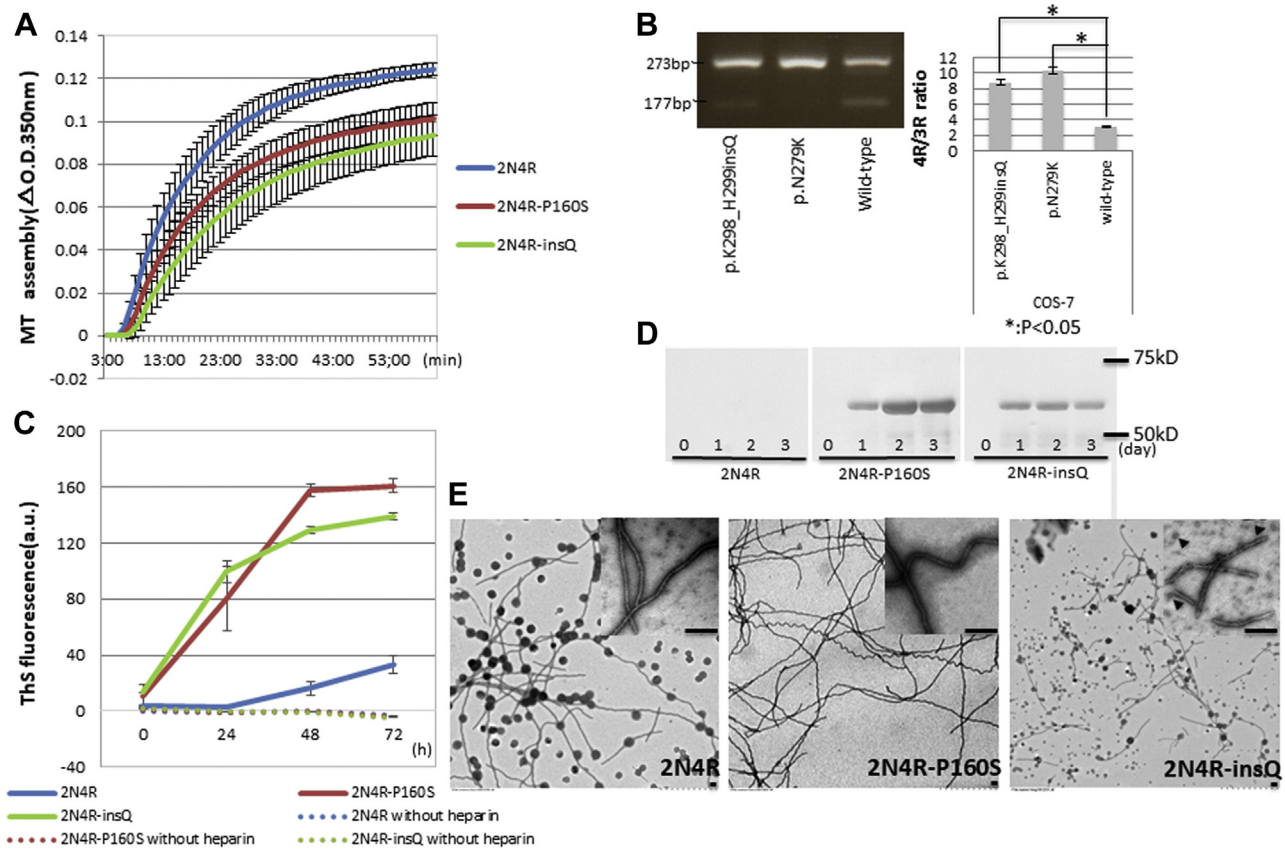

Fig. 2. Biochemical analysis of *p*.P160S and *p*.K298_H299insQ *MAPT* variants. (A) Microtubule assembly assay with recombinant 2N4R, 2N4R-P160S, and 2N4R-insQ ($n = 4$). (B) Exon trapping analysis of variant *p*.K298_H299insQ. The DNA molecule with 273-bp corresponds to 4R-containing exon 10. A 177-bp DNA molecule indicates a lack of exon 10 (3R). Bar graph represents a quantitative analysis of the 4R/3R ratio of wild-type, *p*.N279K, and *p*.K298_H299insQ constructs ($n = 3$). $^{*}p < 0.05$ by Mann-Whitney *U* test. (C) Heparin-induced aggregation activities measured with thioflavin S fluorescence assay ($n = 3$). (D) Sarkosyl-insolubility pattern of heparin-induced aggregation of recombinant 2N4R, 2N4R-P160S, and 2N4R-insQ ($n = 3$). (E) Electron micrographs of tau aggregates of recombinant 2N4R, 2N4R-P160S, and 2N4R-insQ after 7 days of incubation with heparin. Insets in panels show higher magnification images. Black round spots are artifacts. (Arrow heads) round shaped aggregates; bar = 200 nm. Data in the three panels (A–C) represent the mean ± SEM of three or four independent experiments. Abbreviations: MAPT, microtubule-associated protein tau; SEM, standard error of the mean.

aggregates (arrow heads) similar to oligomers. In addition, 2N4R-insQ showed twisted filaments similar to paired helical filaments, with crossover distances ranging from 40 to 80 nm and width ranging from approximately 20 nm at the widest and 15 nm at the narrowest (Fig. 2E).

3.5. *Effects of* MAPT *variants on the aggregation kinetics*

Electron microscopy analysis revealed that heparin-induced recombinant tau aggregates displayed the filament formation. The major component of tau filaments is cross-linked β-sheeted tau. To evaluate the differences in β-sheet formation during heparin-induced aggregation, recombinant 2N4R and the two respective variants were subjected to CD spectroscopy analysis. The CD measurement conditions were slightly different from those of ThS assays, as high concentration of recombinant tau and DTT interferes with the CD measurement of the proteins because of its strong abortion spectra at the far ultraviolet range. We therefore reduced the recombinant concentration to 10 μM and replaced 20 mM DTT with 1.0 mM tris(2-carboxyethyl)phosphine and confirmed that, under the new conditions, tau can form fibrils in the presence of heparin (data not shown). At 0 hours, 2N4R and 2N4R-insQ showed completely overlapping CD spectra, although the 2N4R-P160S spectra had a more negative spectra and a lower negative peak at 207 nm, sensitivity to α-helical structures (Fig. 3A, upper left) (Chen et al., 1972). However, in secondary structure analysis the α-helical structure was only slightly affected (6.5% compared with 5.7% of 2N4R) (Fig. 3C). The value at 217 nm, sensitive to β-structure (a more negative spectrum is indicative of acquisition of more β-structures), gradually became more negative during incubation for all mutants (Fig. 3A, upper right and lower panel, and B). The change was most prominent for 2N4R-insQ. Secondary structure analysis indicated that after 120 hours of incubation 2N4R-insQ had 43.6% of β-structure compared with 26% at the start (Fig. 3D). The amounts of β-structure after 120 hours of incubation for 2N4R and 2N4R-P160S were 32% and 30.5%, respectively. These findings indicated that 2N4R-insQ shows a high aggregation tendency.

3.6. *Effects of* MAPT *variants on the seeding activity of tau*

We compared the seeding activity of aggregated recombinant wild-type tau and variants using a cellular model of intracellular aggregation. Expressed tau was recruited into the Sar-soluble fraction and Sar-insoluble pellet, as detected using the phosphorylation-independent antibody, T46 (Fig. 4A). 2N4R-overexpressing cells with 2N4R-insQ seed showed a significantly higher aggregation in the Sar-insoluble pellet than with 2N4R seed ($p < 0.05$) (Fig. 4A and B, left panels), whereas the T46 immunoreactivities of the Sar-insoluble pellet with the 2N4R-P160S seed were not significantly different. 2N4R-P160S—overexpressing cells showed that the 2N4R-insQ seed induced a significantly increased amount of Sar-insoluble pellet compared with the 2N4R seed ($p <$

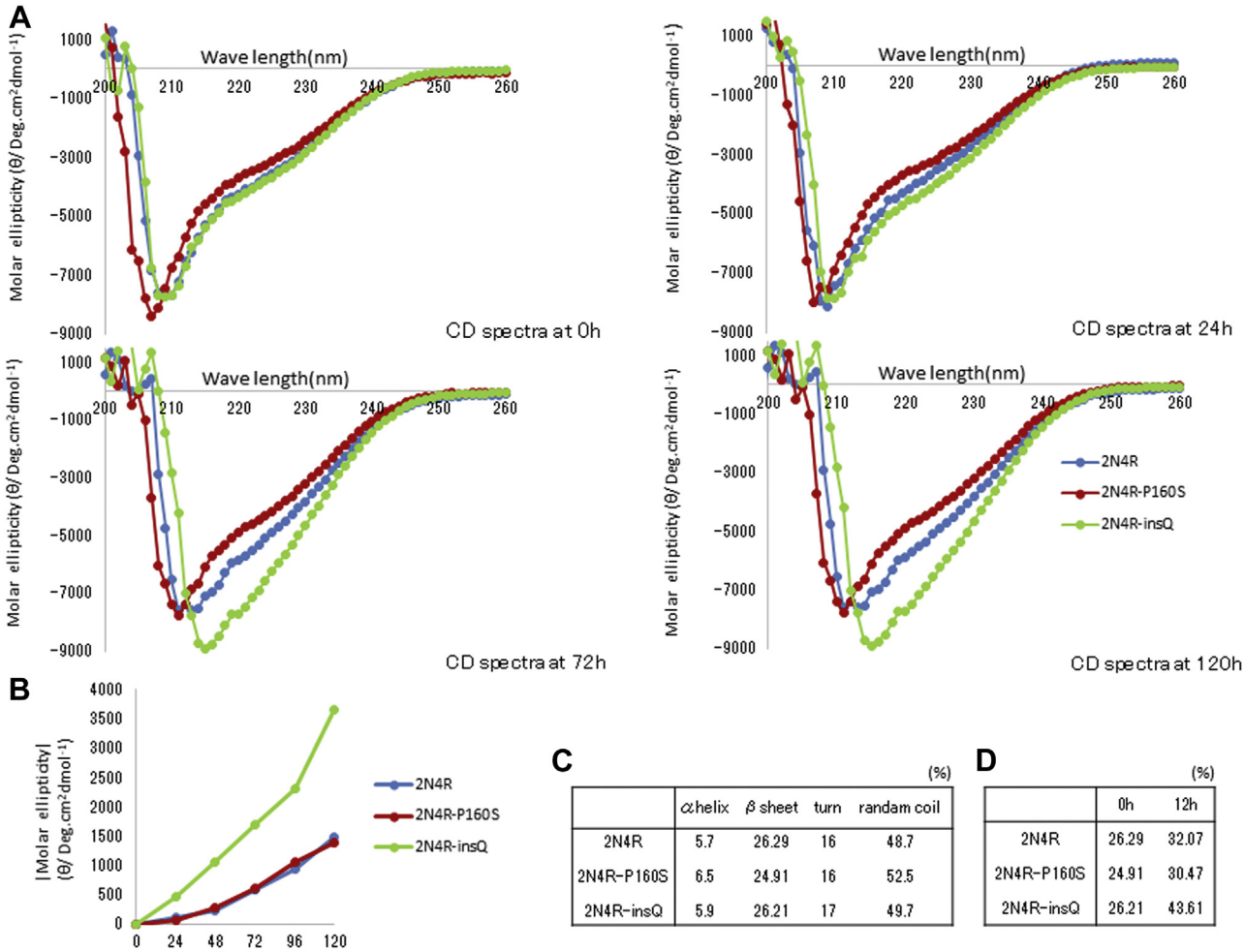

Fig. 3. Tau aggregation analysis of *p*.P160S and *p*.K298_H299insQ *MAPT* variants using Far UV CD. (A) CD spectra of recombinant 2N4R, 2N4R-P160S, and 2N4R-insQ (blue, red, and olive lines, respectively) for 0, 24, 72, and 120 hours of incubation with heparin at 37 °C. CD absorbance spectra were recoded (mdeg) for three different sets of experiments, averaged, standardized against concentration, and converted into molar ellipticity (θ) (deg × cm^2/dmol). (B) Change in the absolute value of molar ellipticity (θ) at 217 nm with incubation time. (C) Analysis of the total secondary structural content of recombinant 2N4R, 2N4R-P160S, and 2N4R-insQ in heparin-induced tau aggregation experiments. (D) A comparative view on time-dependent changes in β-sheet structural content of recombinant 2N4R, 2N4R-P160S, and 2N4R-insQ after 120 hours of incubation at 37 °C with heparin. Abbreviations: CD, circular dichroism; MAPT, microtubule-associated protein tau; UV, ultraviolet. (For interpretation of the references to color in this figure legend, the reader is referred to the Web version of this article.)

0.05) (Fig. 4A and B, middle panels). 2N4R-insQ–overexpressing cells showed a greater amount of insoluble tau in Sar-insoluble pellets from all seeds than those of 2N4R-overexpressing cells or 2N4R-P160S–overexpressing cells (Fig. 4A and B, right panels). This indicated the 2N4R-insQ had the highest aggregation ability in the cell model. Moreover, the 2N4R-insQ seed induced a higher amount of aggregate than the 2N4R or 2N4R-P160S seeds in cells transfected with 2N4R, 2N4R-P160S. These results suggested that seeding activity also depended on the biochemical characteristics of seeds.

To confirm filament formation in the cell, we looked at Sar-insoluble pellets using electron microscopy. Filaments were found in Sar-insoluble pellets from 2N4R-overexpressing cells with either 2N4R or variant seeds (Fig. 4C). The observed filaments were straight, smooth, and gathered in bundles. No difference was observed between wild-type and variant seeds. The morphology of tau filaments in the cell was different from heparin-induced recombinant tau filaments (Fig. 4C).

Fluorescence microscopic examination revealed small tau-positive intracellular puncta in 2N4R-overexpressing cells induced with 2N4R, 2N4R-P160S, and 2N4R-insQ seeds frequently than without seeds (Fig. 5D). PHF-1 positive were detected as small puncta frequently occurring in each cell (Fig. 5A). Some PHF-1 positive puncta were delineated with ThS and tauC staining in the cytoplasm of 2N4R-overexpressing cells with all seeds (Supplementary Fig. 3A and B). Conformation-dependent antibody MC1 and phosphorylation-dependent antibody AT8, which recognizes phospho-Ser 202 and phospho-Thr 205, also immunostained cytoplasmic puncta (Fig. 5B and C).

Quantitative image analysis revealed that 2N4R-P160S and 2N4R-insQ seeds induced a higher number of cells bearing PHF-1 (69.7 ± 9.0% and 75.0 ± 1.83%, respectively) and MC1 (48.8 ± 6.3% and 45.7±2.1%, respectively) positive puncta than 2N4R seed (47.5 ± 5.6% and 32.4 ± 2.1%, respectively, $p < 0.05$) (Fig. 5D). The percentage of puncta-positive cells without seed was 0.62 ± 0.17% (PHF-1) and 14.5 ± 1.9% (MC1). Although similar changes were observed in cells stained with AT8, they were not significant.

4. Discussion

In the present study, we detected two novel heterozygous variants in *MAPT*. One was a missense variant, *p*.P160S in exon 7, in a

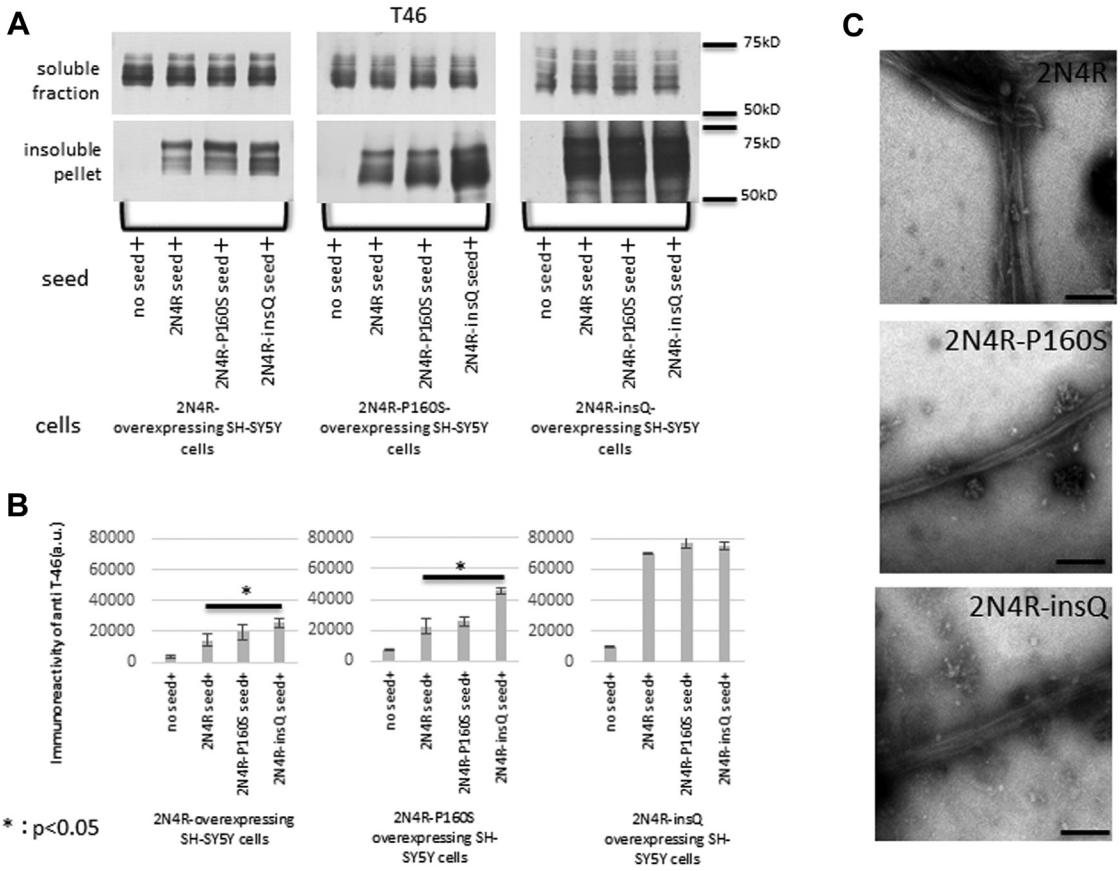

Fig. 4. Seeding activity analysis of 2N4R-P160S and 2N4R-insQ using SH-SY5Y cell models. (A) Tau in sarkosyl-soluble fraction (soluble fraction) or sarkosyl-insoluble pellet (insoluble pellet) from 2N4R-overexpressing, 2N4R-P160S–overexpressing, or 2N4R-insQ–overexpressing cells treated with each seed detected using Tau46 antibody ($n = 3$). (B) Quantitative analysis of immunoreactivity of ppt with cells overexpressing 2N4R, 2N4R-P160S, or 2N4R-insQ. Data represent the mean ± SEM from three independent experiments. $^{*}p < 0.05$ by Student's t test. (C) Electron microscopy of tau filaments in sarkosyl-insoluble pellet extracted from 2N4R-overexpressing cells treated with 2N4R, 2N4R-P160S, or 2N4R-insQ seeds. Bar = 200 nm. Abbreviation: SEM, standard error of the mean.

patient with FTD-MND. The other was an insertion variant, *p*.K298_H299insQ in exon 10, in a case of familial PSP. Our functional analysis indicated that recombinant variant tau reduced microtubule assembly activity and increased the propensity for aggregation in ThS assay. In the cell model, *p*.K298_H299insQ had a higher aggregation ability than wild-type tau, although the aggregation ability of *p*.P160S was the same level as that of wild-type tau. Moreover, the aggregated 2N4R-insQ had a higher seeding activity than that of wild-type tau.

p.K298_H299insQ is the first report of an insertion variant in *MAPT*. Patients harboring variants in *MAPT* exon 10 can be divided into two categories: "dementia-dominant" and "atypical parkinsonism-dominant" such as PSP and CBS (Wszolek et al., 2006). Our case matched atypical parkinsonism-dominant resembling PSP. Recombinant 2N4R-insQ showed a reduced ability of microtubule assembly and increased propensity for aggregation. *p*.K298_H299insQ was detected in MBD as a main functional domain of tau. Inside the MBD, *p*.K298_H299insQ located close to the aggregation-promoting hexapeptide PHF6 (^{306}VQIVYK^{311}) and possibly induces tau aggregation by strengthening PHF6. Several variants (*p*.G303V, *p*.L315R, and *p*.S320F), which may be related to PHF6, display a mixture of short filaments and oligomers (Combs and Gamblin, 2012). These findings are similar to those of *p*.K298_H299insQ, which also suggests that *p*.K298_H299insQ may affect PHF6. Moreover, in exon 10 and flanking introns, multiple *cis*-acting elements regulating exon 10 splicing were identified. The insertion variant located in the *cis*-element, which works as an exon splicing enhancer (Liu and Gong, 2008). The dysregulation of exon splicing enhancer induces an increase in 4R tau. Our exon trapping analysis suggests that the abnormal alternative splicing in exon 10 and the increased expression of 4R tau is caused by *p*.K298_H299insQ. Together, these studies suggest that *p*.K298_H299insQ leads to disruption of normal function of tau and aberrant aggregation in vitro.

Tau aggregates spread through intercellular propagation, requiring the formation of prion-like species (Goedert et al., 2017). The aggregated recombinant tau can work as seeds in previous cell models. The overexpressed tau model without seeds resists aggregation. However, introducing tau seeds into tau-expressing cells generates tau aggregation. We compared the seeding activities of aggregated recombinant tau among 2N4R, 2N4R-P160S, and 2N4R-insQ. 2N4R-insQ seed presented a higher seeding activity than 2N4R and 2N4R-P160S seeds. Moreover, 2N4R-insQ–overexpressing cells showed greater aggregation to various seeds than 2N4R-overexpressing cells. In this cell model, the aggregation propensity of overexpressed tau strongly relates to the seed-induced aggregation (Matsumoto et al., 2015). This indicates that 2N4R-insQ has the highest aggregation ability. On the other hand, the amount of Sar-insoluble pellets of 2N4R-P160S–overexpressing cells was similar to that of 2N4R. The aggregation ability of 2N4R-P160S is not as strong as that of 2N4R-insQ, although similar levels of heparin-induced aggregation were observed in ThS assays. 2N4R-insQ seed induced a higher amount of aggregation than the 2N4R or 2N4R-P160S seeds in cells transfected with 2N4R and 2N4R-P160S.

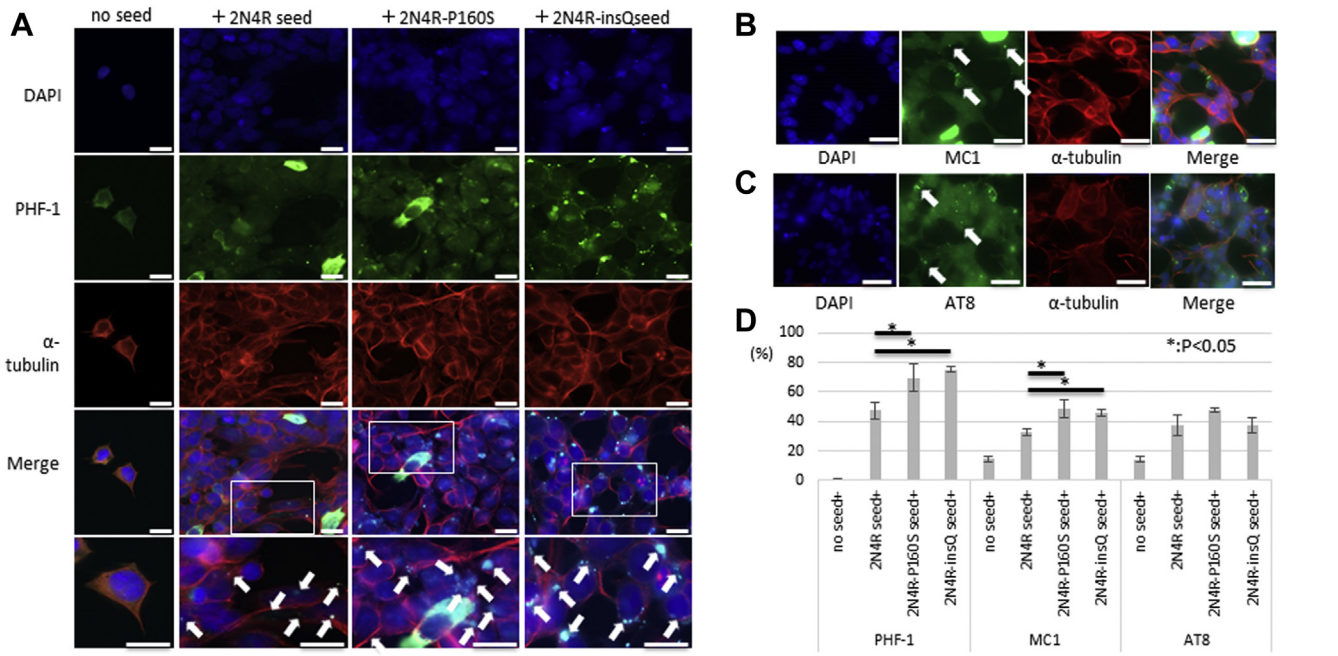

Fig. 5. Immunocytochemical analysis of intracellular tau aggregates induced by various seeds. (A) 2N4R-overexpressing SH-SY5Y cells with 2N4R, 2N4R-P160S, or 2N4R-insQ seed show PHF-1 positive puncta in the cytoplasm. Bar = 50 μm. (B) Triple immunostaining of MC1 antibody in 2N4R-overexpressing cells treated with 2N4R-insQ seed. Bar = 50 μm. (C) Triple immunostaining of AT8 antibody in 2N4R-overexpressing cells treated with 2N4R-P160S seed. Bar = 50 μm. (D) Quantitative analysis of cells containing intracellular puncta decorated with PHF-1, MC1, or AT8 antibodies. The ratios of puncta-containing cells were compared with 2N4R-overexpressing cells with various seeds. Data in panel D represent the mean ± SEM. Each experiment was repeated three times and cells were counted in three views for each experiment. $^{*}p < 0.05$ by Student's *t* test. Abbreviation: SEM, standard error of the mean.

Our CD spectroscopy analysis demonstrated that the ratio of β-sheets is higher in the heparin-induced 2N4R-insQ aggregates than in those of 2N4R and 2N4R-P160S. This suggests that the conformational differences among seeds account for seeding ability (Falcon et al., 2015). Moreover, our experiments showed that seeds of 2N4R-P160S and 2N4R-insQ increased the number of phosphorylated tau-positive puncta and conformationally changed tau-positive puncta in 2N4R-overexpressing cells compared with that of 2N4R seed. *p*.K298_H299insQ and *p*.P160S possibly cause aberrant post-translational modification leading to toxicity.

Our patient with *p*.P160S clinically resembled atypical amyotrophic lateral sclerosis, presenting asymmetrical symptoms afflicting more the upper motor neurons than the lower motor neurons. *p*.P160S located far outside MBD in a proline-rich domain (residues 151-243) (Wang and Mandelkow, 2016). However, a recombinant tau protein with *p*.P160S showed a mildly reduced ability to promote microtubule assembly and enhanced ThS-detected aggregation ability. N-terminal region of the proline-rich domain (residues 151-197), which contains proline 160, is thought not to play a direct role in regulating microtubule dynamics. However, the region contributes to microtubule assembly by assisting in microtubule nucleation and bundle formation (Gustke et al., 1994). Nuclear magnetic resonance spectroscopy reveals that the proline-rich domain mildly interacts with microtubules (Mukrasch et al., 2009). With respect to a high aggregation ability of *p*.P160S, the proline-rich domain forms an intermolecular interaction with the third microtubule binding repeat (R3) (Mukrasch et al., 2009). PHF6 is located at the beginning of R3. Thus, we believe that *p*.P160S may affect PHF6, resulting in enhanced aggregation under high concentration conditions.

Pathogenic variants in *MAPT* are commonly concentrated in exons 9–12 and in introns of exon 10. We detected *p*.P160S in exon 7. In ThS assays of *p*.A152T in the presence of heparin, ThS fluorescence levels were comparable with those of wild-type, and SDS-PAGE quantification of the ThS assembly mixture separated by centrifugation also showed that the rate of aggregated tau was lower than that of wild-type tau. However, microtubule assembly assays clearly demonstrated that *p*.A152T is much less efficient in stabilizing microtubules (Coppola et al., 2012). Our CD spectra and cell-based model assay results show that the aggregation ability of *p*.P160S was the same level of that of wild-type, although *p*.P160S had less ability to promote microtubule assembly than wild-type. We speculate that *p*.P160S and *p*.A152T share pathogenic similarities, with a weak influence on tau aggregation and a decrease in microtubule binding.

This study has several limitations: (1) the small number of patients, (2) autopsies were not performed, and (3) segregation studies were not performed for other family members. To determine the toxicity of both tau protein variants, it is necessary to perform postmortem analyses of autopsied brains. The Japanese Society of Neuropathology has encouraged physicians to persuade patients with neurodegenerative diseases to donate their brains on their passing. We acknowledge that we will encourage the patients and their family members to donate their brains.

5. Conclusions

We detected two novel variants in *MAPT* in patients with FTD-MND and PSP. Our functional analysis demonstrated that recombinant tau modified by two variants revealed a reduced ability of microtubule assembly and an increased ability of aggregation. In a cell-based model, *p*.K298_H299insQ showed a higher aggregation ability and seeding activity compared with wild-type tau. Our characterization of two variants sheds light on tau pathogenesis

and its relationship with MND, progressive parkinsonism, and cognitive decline.

Disclosure

The authors report no conflicts of interest relevant to the manuscript.

Acknowledgements

The authors are grateful to Dr K. Ishiguro for helpful comments on the manuscript. Dr Yumiko Motoi is an Endowed Associate Professor of the Department of Diagnosis, Prevention and Treatment of Dementia and has been sponsored by Nippon Medi-Physics Co Ltd. Dr Nobutaka Hattori has received a speaker honorarium from Nippon Medi-Physics Co Ltd. Dr Nobutaka Hattori and Dr Yumiko Motoi have received research grants from the company. Dr Kenya Nishioka was supported by Japanese Society for the Promotion of Science (JSPS KAKENHI) Grant Number 16K09678.

Appendix A. Supplementary data

Supplementary data associated with this article can be found, in the online version, at https://doi.org/10.1016/j.neurobiolaging.2019.02.016.

References

Adzhubei, I.A., Schmidt, S., Peshkin, L., Ramensky, V.E., Gerasimova, A., Bork, P., Kondrashov, A.S., Sunyaev, S.R., 2010. A method and server for predicting damaging missense mutations. Nat. Methods. 7, 248–249.

American Psychiatric Association, 2013. Diagnostic and Statistical Manual of Mental Disorders, Fifth Edition (DSM-5). American Psychiatric Publishing, Washington, DC.

Andrade, M.A., Chacon, P., Merelo, J.J., Moran, F., 1993. Evaluation of secondary structure of proteins from UV circular dichroism spectra using an unsupervised learning neural network. Protein. Eng. 6, 383–390.

Chen, Y.H., Yang, J.T., Martinez, H.M., 1972. Determination of the secondary structures of proteins by circular dichroism and optical rotatory dispersion. Biochemistry 11, 4120–4131.

Combs, B., Gamblin, T.C., 2012. FTDP-17 tau mutations induce distinct effects on aggregation and microtubule interactions. Biochemistry 51, 8597–8607.

Coppola, G., Chinnathambi, S., Lee, J.J., Dombroski, B.A., Baker, M.C., Soto-Ortolaza, A.I., Lee, S.E., Klein, E., Huang, A.Y., Sears, R., Lane, J.R., Karydas, A.M., Kenet, R.O., Biernat, J., Wang, L.S., Cotman, C.W., Decarli, C.S., Levey, A.I., Ringman, J.M., Mendez, M.F., Chui, H.C., Le Ber, I., Brice, A., Lupton, M.K., Preza, E., Lovestone, S., Powell, J., Graff-Radford, N., Petersen, R.C., Boeve, B.F., Lippa, C.F., Bigio, E.H., Mackenzie, I., Finger, E., Kertesz, A., Caselli, R.J., Gearing, M., Juncos, J.L., Ghetti, B., Spina, S., Bordelon, Y.M., Tourtellotte, W.W., Frosch, M.P., Vonsattel, J.P., Zarow, C., Beach, T.G., Albin, R.L., Lieberman, A.P., Lee, V.M., Trojanowski, J.Q., Van Deerlin, V.M., Bird, T.D., Galasko, D.R., Masliah, E., White, C.L., Troncoso, J.C., Hannequin, D., Boxer, A.L., Geschwind, M.D., Kumar, S., Mandelkow, E.M., Wszolek, Z.K., Uitti, R.J., Dickson, D.W., Haines, J.L., Mayeux, R., Pericak-Vance, M.A., Farrer, L.A., Ross, O.A., Rademakers, R., Schellenberg, G.D., Miller, B.L., Mandelkow, E., Geschwind, D.H., 2012. Evidence for a role of the rare p.A152T variant in MAPT in increasing the risk for FTD-spectrum and Alzheimer's diseases. Hum. Mol. Genet. 21, 3500–3512.

de Carvalho, M., Dengler, R., Eisen, A., England, J.D., Kaji, R., Kimura, J., Mills, K., Mitsumoto, H., Nodera, H., Shefner, J., Swash, M., 2008. Electrodiagnostic criteria for diagnosis of ALS. Clin. Neurophysiol. 119, 497–503.

Di Fonzo, A., Ronchi, D., Gallia, F., Cribiu, F.M., Trezzi, I., Vetro, A., Della Mina, E., Limongelli, I., Bellazzi, R., Ricca, I., Micieli, G., Fassone, E., Rizzuti, M., Bordoni, A., Fortunato, F., Salani, S., Mora, G., Corti, S., Ceroni, M., Bosari, S., Zuffardi, O., Bresolin, N., Nobile-Orazio, E., Comi, G.P., 2014. Lower motor neuron disease with respiratory failure caused by a novel MAPT mutation. Neurology 82, 1990–1998.

Elahi, M., Islam, M.M., Noguchi, K., Yohda, M., Toh, H., Kuroda, Y., 2014. Computational prediction and experimental characterization of a "size switch type repacking" during the evolution of dengue envelope protein domain III (ED3). Biochim. Biophys. Acta. 1844, 585–592.

Falcon, B., Cavallini, A., Angers, R., Glover, S., Murray, T.K., Barnham, L., Jackson, S., O'Neill, M.J., Isaacs, A.M., Hutton, M.L., Szekeres, P.G., Goedert, M., Bose, S., 2015. Conformation determines the seeding potencies of native and recombinant Tau aggregates. J. Biol. Chem. 290, 1049–1065.

Fong, H., Wang, C., Knoferle, J., Walker, D., Balestra, M.E., Tong, L.M., Leung, L., Ring, K.L., Seeley, W.W., Karydas, A., Kshirsagar, M.A., Boxer, A.L., Kosik, K.S., Miller, B.L., Huang, Y., 2013. Genetic correction of tauopathy phenotypes in neurons derived from human induced pluripotent stem cells. Stem. Cell. Reports. 1, 226–234.

Forrest, S.L., Kril, J.J., Stevens, C.H., Kwok, J.B., Hallupp, M., Kim, W.S., Huang, Y., McGinley, C.V., Werka, H., Kiernan, M.C., Gotz, J., Spillantini, M.G., Hodges, J.R., Ittner, L.M., Halliday, G.M., 2018. Retiring the term FTDP-17 as MAPT mutations are genetic forms of sporadic frontotemporal tauopathies. Brain 141, 521–534.

Goedert, M., Eisenberg, D.S., Crowther, R.A., 2017. Propagation of tau aggregates and neurodegeneration. Annu. Rev. Neurosci. 40, 189–210.

Gorno-Tempini, M.L., Hillis, A.E., Weintraub, S., Kertesz, A., Mendez, M., Cappa, S.F., Ogar, J.M., Rohrer, J.D., Black, S., Boeve, B.F., Manes, F., Dronkers, N.F., Vandenberghe, R., Rascovsky, K., Patterson, K., Miller, B.L., Knopman, D.S., Hodges, J.R., Mesulam, M.M., Grossman, M., 2011. Classification of primary progressive aphasia and its variants. Neurology 76, 1006–1014.

Gustke, N., Trinczek, B., Biernat, J., Mandelkow, E.M., Mandelkow, E., 1994. Domains of tau protein and interactions with microtubules. Biochemistry 33, 9511–9522.

Hasegawa, M., Crowther, R.A., Jakes, R., Goedert, M., 1997. Alzheimer-like changes in microtubule-associated protein Tau induced by sulfated glycosaminoglycans. Inhibition of microtubule binding, stimulation of phosphorylation, and filament assembly depend on the degree of sulfation. J. Biol. Chem. 272, 33118–33124.

Hasegawa, M., Smith, M.J., Iijima, M., Tabira, T., Goedert, M., 1999. FTDP-17 mutations N279K and S305N in tau produce increased splicing of exon 10. FEBS. Lett. 443, 93–96.

Higasa, K., Miyake, N., Yoshimura, J., Okamura, K., Niihori, T., Saitsu, H., Doi, K., Shimizu, M., Nakabayashi, K., Aoki, Y., Tsurusaki, Y., Morishita, S., Kawaguchi, T., Migita, O., Nakayama, K., Nakashima, M., Mitsui, J., Narahara, M., Hayashi, K., Funayama, R., Yamaguchi, D., Ishiura, H., Ko, W.Y., Hata, K., Nagashima, T., Yamada, R., Matsubara, Y., Umezawa, A., Tsuji, S., Matsumoto, N., Matsuda, F., 2016. Human genetic variation database, a reference database of genetic variations in the Japanese population. J. Hum. Genet. 61, 547–553.

Ioannidis, N.M., Rothstein, J.H., Pejaver, V., Middha, S., McDonnell, S.K., Baheti, S., Musolf, A., Li, Q., Holzinger, E., Karyadi, D., Cannon-Albright, L.A., Teerlink, C.C., Stanford, J.L., Isaacs, W.B., Xu, J., Cooney, K.A., Lange, E.M., Schleutker, J., Carpten, J.D., Powell, I.J., Cussenot, O., Cancel-Tassin, G., Giles, G.G., MacInnis, R.J., Maier, C., Hsieh, C.L., Wiklund, F., Catalona, W.J., Foulkes, W.D., Mandal, D., Eeles, R.A., Kote-Jarai, Z., Bustamante, C.D., Schaid, D.J., Hastie, T., Ostrander, E.A., Bailey-Wilson, J.E., Radivojac, P., Thibodeau, S.N., Whittemore, A.S., Sieh, W., 2016. REVEL: an Ensemble method for predicting the pathogenicity of rare missense variants. Am. J. Hum. Genet. 99, 877–885.

Irwin, D.J., Cairns, N.J., Grossman, M., McMillan, C.T., Lee, E.B., Van Deerlin, V.M., Lee, V.M., Trojanowski, J.Q., 2015. Frontotemporal lobar degeneration: defining phenotypic diversity through personalized medicine. Acta. Neuropathol. 129, 469–491.

Kircher, M., Witten, D.M., Jain, P., O'Roak, B.J., Cooper, G.M., Shendure, J., 2014. A general framework for estimating the relative pathogenicity of human genetic variants. Nat. Genet. 46, 310–315.

Lek, M., Karczewski, K.J., Minikel, E.V., Samocha, K.E., Banks, E., Fennell, T., O'Donnell-Luria, A.H., Ware, J.S., Hill, A.J., Cummings, B.B., Tukiainen, T., Birnbaum, D.P., Kosmicki, J.A., Duncan, L.E., Estrada, K., Zhao, F., Zou, J., Pierce-Hoffman, E., Berghout, J., Cooper, D.N., Deflaux, N., DePristo, M., Do, R., Flannick, J., Fromer, M., Gauthier, L., Goldstein, J., Gupta, N., Howrigan, D., Kiezun, A., Kurki, M.I., Moonshine, A.L., Natarajan, P., Orozco, L., Peloso, G.M., Poplin, R., Rivas, M.A., Ruano-Rubio, V., Rose, S.A., Ruderfer, D.M., Shakir, K., Stenson, P.D., Stevens, C., Thomas, B.P., Tiao, G., Tusie-Luna, M.T., Weisburd, B., Won, H.H., Yu, D., Altshuler, D.M., Ardissino, D., Boehnke, M., Danesh, J., Donnelly, S., Elosua, R., Florez, J.C., Gabriel, S.B., Getz, G., Glatt, S.J., Hultman, C.M., Kathiresan, S., Laakso, M., McCarroll, S., McCarthy, M.I., McGovern, D., McPherson, R., Neale, B.M., Palotie, A., Purcell, S.M., Saleheen, D., Scharf, J.M., Sklar, P., Sullivan, P.F., Tuomilehto, J., Tsuang, M.T., Watkins, H.C., Wilson, J.G., Daly, M.J., MacArthur, D.G., Exome Aggregation Consortium, 2016. Analysis of protein-coding genetic variation in 60,706 humans. Nature 536, 285–291.

Lindquist, S.G., Holm, I.E., Schwartz, M., Law, I., Stokholm, J., Batbayli, M., Waldemar, G., Nielsen, J.E., 2008. Alzheimer disease-like clinical phenotype in a family with FTDP-17 caused by a MAPT R406W mutation. Eur. J. Neurol. 15, 377–385.

Litvan, I., Agid, Y., Calne, D., Campbell, G., Dubois, B., Duvoisin, R.C., Goetz, C.G., Golbe, L.I., Grafman, J., Growdon, J.H., Hallett, M., Jankovic, J., Quinn, N.P., Tolosa, E., Zee, D.S., 1996. Clinical research criteria for the diagnosis of progressive supranuclear palsy (Steele-Richardson-Olszewski syndrome): report of the NINDS-SPSP international workshop. Neurology 47, 1–9.

Liu, F., Gong, C.X., 2008. Tau exon 10 alternative splicing and tauopathies. Mol. Neurodegener. 3, 8.

Maeda, S., Djukic, B., Taneja, P., Yu, G.Q., Lo, I., Davis, A., Craft, R., Guo, W., Wang, X., Kim, D., Ponnusamy, R., Gill, T.M., Masliah, E., Mucke, L., 2016. Expression of A152T human tau causes age-dependent neuronal dysfunction and loss in transgenic mice. EMBO. Rep. 17, 530–551.

Mathew, R., Bak, T.H., Hodges, J.R., 2012. Diagnostic criteria for corticobasal syndrome: a comparative study. J. Neurol. Neurosurg. Psychiatry. 83, 405–410.

Matsumoto, S.E., Motoi, Y., Ishiguro, K., Tabira, T., Kametani, F., Hasegawa, M., Hattori, N., 2015. The twenty-four KDa C-terminal tau fragment increases with

aging in tauopathy mice: implications of prion-like properties. Hum. Mol. Genet. 24, 6403–6416.
Mukrasch, M.D., Bibow, S., Korukottu, J., Jeganathan, S., Biernat, J., Griesinger, C., Mandelkow, E., Zweckstetter, M., 2009. Structural polymorphism of 441-residue tau at single residue resolution. PLoS Biol. 7, e34.
Mukrasch, M.D., Biernat, J., von Bergen, M., Griesinger, C., Mandelkow, E., Zweckstetter, M., 2005. Sites of tau important for aggregation populate (beta)-structure and bind to microtubules and polyanions. J. Biol. Chem. 280, 24978–24986.
Ng, A.S., 2015. Genetics of frontotemporal dementia in Asia: advancing knowledge through collaboration. Neurology 85, 2060–2062.
Nonaka, T., Watanabe, S.T., Iwatsubo, T., Hasegawa, M., 2010. Seeded aggregation and toxicity of {alpha}-synuclein and tau: cellular models of neurodegenerative diseases. J. Biol. Chem. 285, 34885–34898.
Olszewska, D.A., Lonergan, R., Fallon, E.M., Lynch, T., 2016. Genetics of frontotemporal dementia. Curr. Neurol. Neurosci. Rep. 16, 107.
Rascovsky, K., Hodges, J.R., Knopman, D., Mendez, M.F., Kramer, J.H., Neuhaus, J., van Swieten, J.C., Seelaar, H., Dopper, E.G., Onyike, C.U., Hillis, A.E., Josephs, K.A., Boeve, B.F., Kertesz, A., Seeley, W.W., Rankin, K.P., Johnson, J.K., Gorno-Tempini, M.L., Rosen, H., Prioleau-Latham, C.E., Lee, A., Kipps, C.M., Lillo, P., Piguet, O., Rohrer, J.D., Rossor, M.N., Warren, J.D., Fox, N.C., Galasko, D., Salmon, D.P., Black, S.E., Mesulam, M., Weintraub, S., Dickerson, B.C., Diehl-Schmid, J., Pasquier, F., Deramecourt, V., Lebert, F., Pijnenburg, Y., Chow, T.W., Manes, F., Grafman, J., Cappa, S.F., Freedman, M., Grossman, M., Miller, B.L., 2011. Sensitivity of revised diagnostic criteria for the behavioural variant of frontotemporal dementia. Brain 134 (Pt 9), 2456–2477.
Schwarz, J.M., Cooper, D.N., Schuelke, M., Seelow, D., 2014. MutationTaster2: mutation prediction for the deep-sequencing age. Nat. Methods. 11, 361–362.
Wada-Isoe, K., Ito, S., Adachi, T., Yamawaki, M., Nakashita, S., Kusumi, M., Hiroe, Y., Takada, T., Watanabe, K., Hikasa, C., Nakashima, K., 2012. Epidemiological survey of frontotemporal lobar degeneration in tottori prefecture, Japan. Demen. Geriatr. Cogn. Disord. Extra. 2, 381–386.
Wang, Y., Mandelkow, E., 2016. Tau in physiology and pathology. Nat. Rev. Neurosci. 17, 5–21.
Wszolek, Z.K., Tsuboi, Y., Ghetti, B., Pickering-Brown, S., Baba, Y., Cheshire, W.P., 2006. Frontotemporal dementia and parkinsonism linked to chromosome 17 (FTDP-17). Orphanet. J. Rare. Dis. 1, 30.